Pressure Drop Measurements in a Microchannel

David Pfund, David Rector, and Alireza Shekarriz
Pacific Northwest National Laboratory, Richland, WA 99352

Aristotel Popescu and James Welty
Dept. of Mechanical Engineering, Orgeon State University, Corvallis, OR 97331

Recent developments in micro-energy and micro-chemical systems have produced a need for greater understanding of flow in small channels. Several recent studies of friction factors and transition Reynolds numbers in rectangular microchannels have produced results that differ from classical theory. In this work, friction factors and laminar flow friction constants were determined for water flowing in high aspect ratio channels with depths ranging from 128 to 521 μm. Reynolds numbers were between 60 and 3,450. Pressure drops were measured within the channel itself to exclude entrance and exit losses. Transitions to turbulence were observed with flow visualization. Uncertainties in measured variables were quantified and propagated into the estimated friction constants. Friction factors were also determined in a 1,050-μm-deep channel that served as a control. After considering experimental uncertainties and systematic errors, significant differences remained between the results and classical theory.

Introduction

Rapid advances in microelectronics during the past two decades have brought about a surge of interest in identifying means to reject heat from small surfaces. Heat fluxes in excess of 100 W/cm^2 are often required and in some instances rates that are an order of magnitude higher are desirable. A number of studies have been performed on this topic where the authors concluded that single-phase microchannel cooling can be used as an effective means of heat rejection (Knight et al., 1992; Kleiner et al., 1995). Additionally, for the development of microelectromechanical systems (MEMS), and micro-energy and chemical systems (MECS), flow through small channels and passages is almost always required. Given the growing dependence on flow through microchannels, there are a number of gaps that currently appear to exist in the knowledge-base regarding these flows.

Pfahler et al. (1990a,b) posed the four important questions (which follow in paraphrased form) that have been asked repeatedly in subsequent studies of flow in microchannels: (a) At what length scales do continuum assumptions become inappropriate?; (b) Do the Navier-Stokes equations model the flow?; (c) Are typically ignored factors important in small channels?; (d) Is the onset of instability affected by the small channel size? Experimental and analytical investigations of gaseous flow in microchannels have shown that rarefraction and compressibility effects appear in such flows (Arkilic et al., 1997). Experiments that have attempted to answer Pfahler's questions for liquid flows have produced contradictory results. While not attempting to answer these questions directly, the objective of this work is to eliminate some of this confusion by carefully identifying and controlling experimental variables, and by augmenting measurements of pressure drop with visualization of the flow regime.

Some studies have reported friction factors that were greater than classical. Wu and Little (1983) measured friction factors in laminar and in turbulent flow of gas flowing in channels etched into silicon and abraded into glass. They found friction factors to be greater than the classical values, although they made their comparison to the Moody Chart for flow in round pipes, not to corresponding charts for rectangular ducts. Pfahler et al. (1990a) found friction factors in laminar flow of n-propanol in a 0.8 μm deep by 100-μm wide channel to be greater than theoretical values.

A more common result was to find friction factors for flow in microchannels that were less than those predicted from classical hydrodynamics. Cuta et al. (1996) found that friction

Correspondence concerning this article should be addressed to D. Pfund.

factors for laminar flow of refrigerant R-124 were less than classical, although once again the comparison was made to friction factors for pipe flow. Pfahler et al. (1990b) found, in studies using nitrogen gas, n-propanol, and silicone oil liquids, that friction factors in laminar flow in microchannels were consistently less than theory. Yu et al. (1995) examined laminar flow of nitrogen and water in smooth microtubes with diameters of 19.6 to 102 μm. They found that the friction constant $f \cdot Re$ was significantly less than the classical value of 64. They also concluded that friction factors in turbulent flow were less than the classical values for flow in smooth tubes.

Some studies have reported friction factors that were less than classical values in some cases, and greater than these values in other cases. Peng et al. (1994a,b) examined the flow of water in rectangular channels for several depths and aspect ratios. They observed that only over a special range of height to width (H/W) ratio were friction factors less than classical. The difference between the cases was presumed to be the result of channel geometry or hydraulic diameter effects that are not yet understood. Differences between experimental and theoretical values were found to increase as the dimensions of the channel were reduced.

A few articles have reported more radical differences between theory and experiments on laminar flows in microchannels. Pfahler et al. (1990b) reported that $f \cdot Re$ for the flow of silicone oil was not constant, as the classical theory requires (although they found it to be so for *n*-propanol and for nitrogen gas). They note, however, that the fluid was non-Newtonian and that they did not measure channel depths with sufficient accuracy to conclude that $f \cdot Re$ was significantly different than the classical value. Peng et al. (1994a) reported that laminar friction factors for water were proportional to $Re^{-1.98}$, a result that is not supported by the bulk of the literature. All other studies have reported laminar friction factors that were proportional to Re^{-1}.

There is general agreement in the literature that the high relative roughness of microchannels reduces the critical Reynolds number for transition to turbulent flow. It is well known that roughness influences the transition to turbulence (Schlichting, 1979). Wu and Little (1983) observed that the transition from laminar to turbulent flow (as indicated by a break in the friction factor from the laminar flow line) occurred at a lower Reynolds number in rougher abraded glass channels than in etched silicon channels. They found transitions to occur at Reynolds numbers as low as 400. Peng et al. (1994a,b) detected transitions to turbulence at Reynolds numbers between 200 and 700, with the transition value being dependent on the hydraulic diameter. They also noted that the apparent size of the transition region was reduced as hydraulic diameter was reduced. Curiously, they never observed a fully developed, constant friction factor even though the microchannels, which were machined into stainless steel, were presumably very rough. None of these studies attempted visualization of the flow.

The unusual results reported above have been attributed to several factors, the principal ones being channel size/hydraulic diameter, channel geometry/aspect ratio, relative roughness and asymmetric roughness, and fluid species. Unfortunately, these studies typically left many of the experimental variables unmeasured, uncontrolled, or not varied systematically. Thus, no firm conclusions can be reached about the hypothesized factors. Invariably, these studies have not measured pressures within the microchannel itself, but have instead measured the pressures far upstream and downstream of the channel, as well as applied unexplained corrections for the inlet and exit losses. As microchannels typically have complex entrances and exits, and velocity profiles at the inlets are unknown, a procedure that applies *a priori* corrections is likely to fail. The exception to this is the work of Pong et al. (1994) who measured pressures of flowing gas with microsensors that were integrated with the channel. They found pressure to be nonlinear with distance from the inlet, which in their case was ascribed to compressibility and Knudsen number effects. Although surface roughness is important, it has not been well characterized or varied systematically. Where roughness measurements have been made in addition to flow measurements (Pfahler et al., 1990b), they have been done using one-dimensional (1-D) profilometry of only a few sections of the channel. In the only study where roughness was varied (Wu and Little, 1983) the values of relative roughness were inferred by reference to von Kármán's equation for turbulent friction factors in rough pipes. As has been noted by Pfahler et al. (1990b), accurate measurements of the depth of the microchannel are extremely important to obtain accurate values of the friction constant $f \cdot Re$. The error in the constant is at least triple the error in the depth. For channels that are "micro" in two dimensions, the affect is even worse. As yet, no one has attempted to measure channel dimensions across the width and down the length of an assembled microchannel, as would be needed to estimate any variation of or uncertainty in the channel depth. Noise in the friction factor data, combined with a limited number of data points can make determination of functional relationships uncertain (Cuta et al., 1996). As the transition to turbulent flow has been inferred by a jump in the friction factor, any noise in the friction factor (or in the Reynolds number) adds uncertainty to the width of the transition zone. Finally, where authors have presented unusual exponents on the Reynolds number (Peng et al., 1994a), they have not presented confidence intervals on these estimates. It has not been demonstrated that the exponents are significantly different from unity. When the transition Reynolds number is determined by the intersection of two such curve fits laid in the midst of a plot of scattered data (Peng et al., 1994a), the result is unreliable.

In this work, attempts have been made to incorporate the best features of past work while trying to eliminate the shortcomings. Friction factors were measured in wide microchannels, maintaining a high aspect ratio as channel depth was varied. The channel surfaces are removable, and were characterized with 2-D profilometry. Channel depths were measured *in situ* at multiple points along the width and length of the channel. Pressure drops were measured within the channel, away from the entrance and exit. Large numbers of data points were collected at each flow rate, so that mean values could be determined accurately. Standard deviations were determined for each of the measured variables, and the resulting uncertainties were applied to the calculated values of $f \cdot Re$. The transition Reynolds number, suggested by a plot of $f \cdot Re$ vs. Re, was verified by with a Reynolds dye experiment (using video photomicroscopy) for one case.

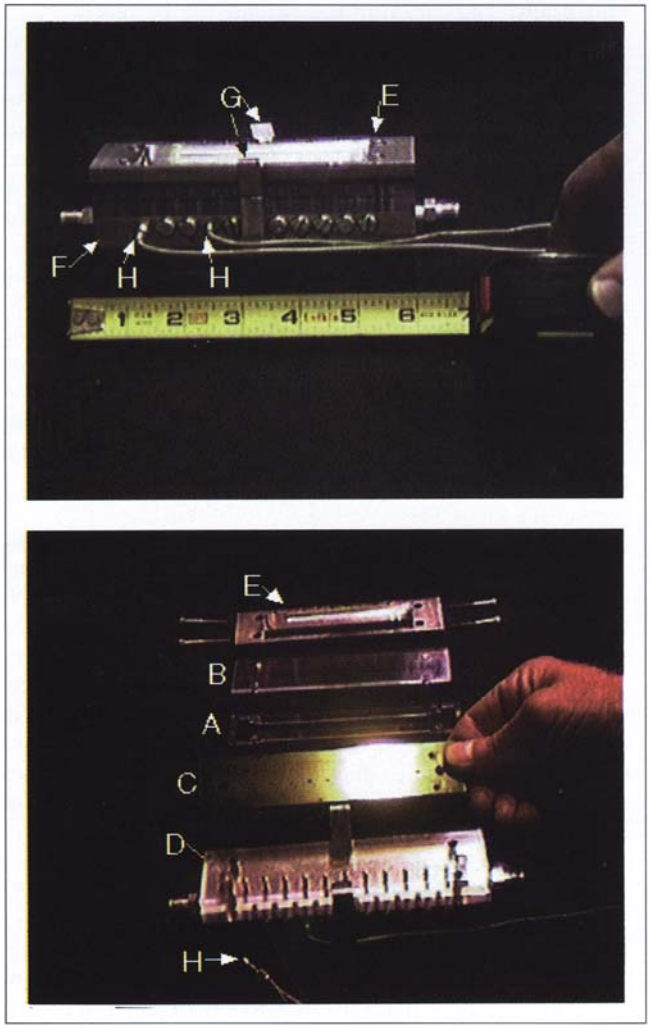

Figure 1. Test section.

Assembled (top), disassembled (bottom).

Experimental Studies

Description of test section

The test section was designed to yield accurate measurements of the friction factor, and to allow flow visualization. The test section was made in a sandwich structure, which is shown assembled and disassembled in the top and bottom, respectively, of Figure 1. A single microchannel was formed by a spacer/gasket (item A in the figure) which was sandwiched between a clear 1/8-in. thick polycarbonate top (B) and a 0.05-in. thick polyimide (DuPont CIRLEX film) bottom plate (C). The fluid within the channel was viewed through the clear top. The thickness of the spacer, and, therefore, the depth of the channel, was varied between 128 μm and 1,050 μm, to allow the progression from microchannel to near macrochannel flow to be examined. The width of the channel cut into each spacer was fixed at 1 cm. The wide channel gave an approximately 2-D flow, thereby simplifying the theoretical description of the flow. The sandwich rested on a support plate made from 1/2-in. thick polycarbonate plastic (D). The whole assembly was held together between a stainless steel top and bottom pressure plates (E and F, respectively) by screws and a clamping mechanism (G). The polycarbonate support plate and the bottom pressure plate were drilled with passageways for fluid inlet and outlet, and for pressure taps. A series of eleven pressure taps (0.5 mm in diameter), spaced at 1.016 cm intervals, were placed along the base of the channel. The taps allowed measurement of pressures within the channel, far away from the inlet and exit. The microchannel was 10 cm long, so that the flow profile would be fully developed within at least the middle third of the channel's length, when a spacer of microchannel thickness was installed. The pressure drop across selected portions of the channel was measured with two miniature sensors (items H in Figure 1). Pressure drops associated with entrance and exit effects were measured and excluded from the determination of friction factor.

Microchannel depths

The sandwich construction allowed a variety of channel depths to be studied by changing the thickness of the spacer. The other dimensions of the channel did not change when the spacer was changed. Microchannels with mean depths ($\overline{H}$) of 521 μm, 263 μm, and 128 μm were assembled with a smooth polyimide bottom plate. A macroscale control with a mean depth of 1,050 μm was also assembled with the smooth plate. A rough polyimide bottom plate was used in a channel that had a mean depth of 257 μm. The surface characteristics of the top and bottom plates are discussed below. An effort was made to accurately measure the depths of the channels *in situ*. Mean channel depths were measured with the test section mounted on a vertically translating stage with a micrometer adjustment and the assembly placed under a microscope. The measurements were made using a 10X, NA (numerical aperture) = 0.25 objective lens. This objective gave a photographic depth of field of approximately 8.5 μm, and visual depth of field of approximately 25 μm (Delly, 1988). The microscope's optics were aligned, and the illumination apertures were stopped down to allow the sharpest focus. The microscope was focused on the top and bottom surfaces of the microchannel, and the channel depths were determined from the differences in micrometer readings. The field stop was stopped down during measurements to improve contrast. Final focusing was made on a video image obtained from a camera mounted on the microscope. For all cases except the 128-μm deep channel, the microchannel was pressurized with water at approximately 2 bar gauge pressure. The measured micrometer readings were then multiplied by the refractive index of water to arrive at the depth of the channel (a paraxial approximation). Measurements were made at 9 points along the channel centerline and at 9 more approximately 2 mm away from the wall. Mean channel depths and confidence intervals on the mean at the 95% confidence level are listed in Table 1. Also listed in Table 1 are the estimated standard deviations of the particular measurements σ_H and the estimated standard deviations in the mean of the measurements $\sigma_{\overline{H}}$ (Mendenhall and Sincich, 1984). In general, the mean channel depth was measured to within $+/-$ 5 to 8 μm, depending on the configuration. There was no indication of bowing or sagging in the microchannels, although the relatively large values of σ_H would have obscured any such irregularity.

Table 1. Channel Depth Measurements

Spacer Thickness μm	Bottom Plate Surface	Mean Depth $\overline{H} \pm \delta\overline{H}$, μm	Std. Dev. of Depth Observed σ_H, μm	Std. Dev. of Mean Depth $\sigma_{\overline{H}}$, μm	Number of Observations N
1,016	Smooth	$1{,}050 \pm 6$	18.4	3.1	36
508	Smooth	521 ± 8	16.8	4.0	18
254	Smooth	263 ± 8	15.8	3.7	18
254	Rough	257 ± 7	14.5	3.4	18
127	Smooth	128 ± 5	9.9	2.3	18

Microchannel surface roughness

The sandwich construction of the test section and the relative ease with which it could be assembled and disassembled allowed the channel walls to be replaced by new walls that were roughened to a specified degree. Surface profilometry was performed on the disassembled parts, without the need for destructive testing. Surface roughness of the top polycarbonate and bottom polyimide plates was measured with a white light interferometer (Zygo New View 200 Optical Profilometer). The instrument allowed noncontact profilometry with 5-Angstrom vertical resolution and 1.1 μm lateral resolution. In addition to providing quantitative measures of the sizes of surface features, the instrument provided false color images of selected portions of the surface. Plan and section views for the top plate and for the smooth and rough bottom plates are given in Figure 2. The mean amplitude of roughness on the polycarbonate top plate was $+/-0.16$ μm, with a maximum peak-valley height of 2.35 μm. The top plate was covered with approximately $0.5-$ μm deep scratches that were parallel to the flow axis. The scratches were spaced across the channel at roughly 25—45 μm intervals. The mean amplitude of roughness on the smooth polyimide bottom plate was $+/-$ 0.09 μm, with a maximum peak-valley height of 2.99 μm. The smooth polyimide plate was used with the surface condition as received from the supplier, with no additional polishing, and was not scratched. The mean amplitude of roughness on the rough polyimide bottom plate was $+/-$ 1.90 μm, with a maximum peak-valley height of approximately 14.67 μm. The surface of the rough polyimide was covered with a crosshatch of scratches resulting from it having been sanded with (''LP2 FINE'' grade) emery cloth. The scratches were roughly 3-μm deep, spaced 100—400 μm apart.

Flow system

The test section was installed in a high-turndown, low noise, water flow system, as shown in Figure 3. The once-through system was driven by water main pressure and did not use a pump. Water entered the system through a pressured pulsation damper with a volume of approximately 19 L and an air-reservoir pressure of 2-bar gauge. From there, it flowed through a de-ionization column and into a set of manual valves which were used to control the pressure of the experiment. The valves were adjusted to control the pressure at the downstream pressure sensor in the test section by varying a bleed flow to a drain. Each experiment was run at an approximately constant downstream pressure, within the range of 1.75 to 2.70 bar gauge. Before entering the test section, the water flowed through a filter with a nominal pore size of 1.6-μm (Glass Microfibre Filters, from Whatman, Inc.). The filter was specified to remove 98% of particles larger than 1.6-μm, to protect downstream equipment. Low water supply pressures prevented the use of smaller pore, higher-pressure drop, filters. Examination of filtered water under a microscope, using both bright and dark field illumination, showed that no particles were present (larger than the resolution limit of $1-$ μm). After leaving the test section, water flowed into a manifold of three needle metering valves (one Nupro model SS-SS4-EP-VH and two Nupro SS-4MG-EP-MH valves) that were used to control the flow rate in the range between 15 and 1,000 mL/min. The resulting pressure drops through the test section were 0.95 bar gauge or less. The temperature of the water leaving the system was measured with a thermocouple probe. Water temperatures varied over a narrow range between 21°C and 24°C.

As discussed above, the pressures within the test section were measured with a pair of miniature pressure sensors, Endevco models 8510C-100 (range 0—6.89 bar gauge) and 8510C-50 (range 0—3.45 bar gauge), each having a manufacturer's claimed nonrepeatability of 0.1% of full scale. The sensors featured self-contained temperature compensation. Both sensors were calibrated with compressed air using a temperature compensated, 0—100 psi range Heise gauge. The bodies of the transducers were threaded into ports in the bottom stainless steel pressure plate that formed the bottom of the clamping mechanism. These ports fed into those in the 1/2-in. thick polycarbonate support plate and from there in turn into (0.5 mm in diameter) taps in the polyimide base of the channel. By running each experiment at an approximately constant pressure, the offset between the two sensors was held constant, enabling it to be measured and subtracted from the pressure drop readings. The test section was grounded to the signal conditioning unit to reduce 60 Hz noise in the indicated pressure.

Flow rates were measured using miniature turbine meters with high turndown-McMillan models 102-3P (with a range of 15 to 100 mL/minute of water) and 102-6P (with a range of 100 to 1,000 mL/min of water). The meters were supplied with NIST-traceable calibration and had a specified accuracy of 1% of full scale. These meters were checked by flowing water into beakers placed on a balance, and comparing the totaled readings to the collected volume at 12—13 points for each meter. The uncertainty in the calibration curve for the model 102-3P meter was $+/-0.2$ mL/min (at the 95% confidence level). High errors were concentrated at the low limit of the model 102-3P's range and errors decreased in magnitude with increasing flow. The uncertainty in the curve for

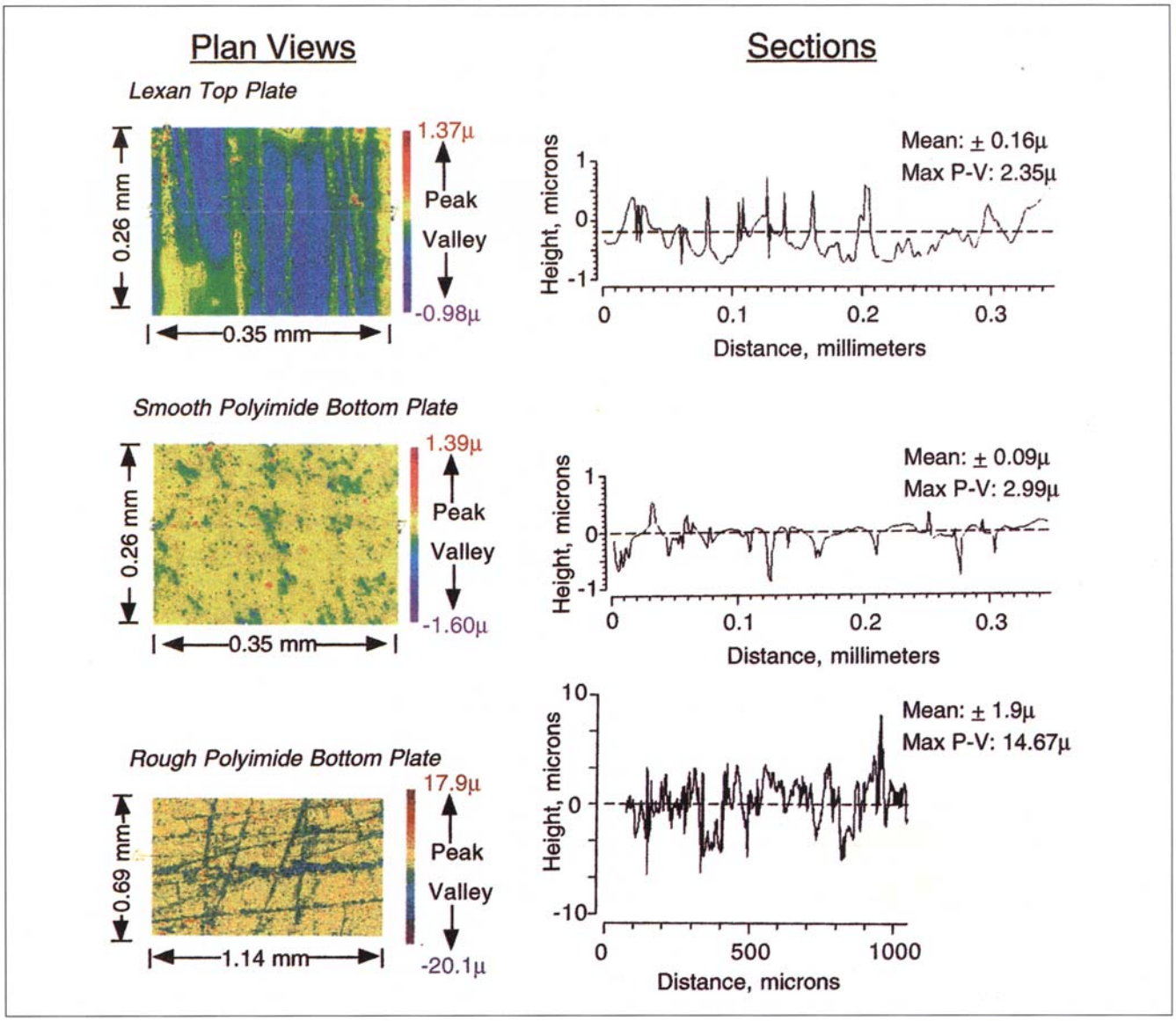

Figure 2. Profilometer images of top and bottom channel surfaces.

the model 102-6P was +/−3.2 mL/min. High errors were distributed over the whole range of flows, with the model 102-6P sometimes reading high, sometimes reading low. Percentage errors, of course, decreased with increasing flow. The uncertainty in individual measurements was +/−0.6 mL/min for the model 102-3P, and +/−11.5 mL/min for the model 102-6P.

Data acquisition

Pressures and flow rates were logged on a computer. Each pressure sensor was connected to a transmitter (Absolute Process Instruments Inc., model API 4059G strain gauge to DC transmitters). Signals from the transmitters and from the turbine flow meter were acquired by a data acquisition card (Analog Connection PC model ACPC-12-16) installed in a personal computer. Data acquisition software (WorkBench PC from Strawberry Tree Inc.) performed the data collection, averaging and logging. Between 10 and 1,000 measurements were made per second. Readings were sample averaged for intervals of one second in length and the averages were logged to the computer's hard disk every second.

Experimental procedure

Before each experiment, the test section was assembled with the desired polyimide bottom plate and polycarbonate spacer. Changing the bottom plate varied surface conditions; changing the spacer varied the channel depth. The bottom plate was sealed to the 1/2-in. thick polycarbonate support plate, and the latter was in turn sealed to the stainless steel bottom pressure plate, with thin layers of silicone vacuum grease. Sealant was not needed on the spacer. Air was bled from the system, with particular attention being paid to remove air from the pressure tap ports (trapped air was found to induce noise in the measured pressure drop).

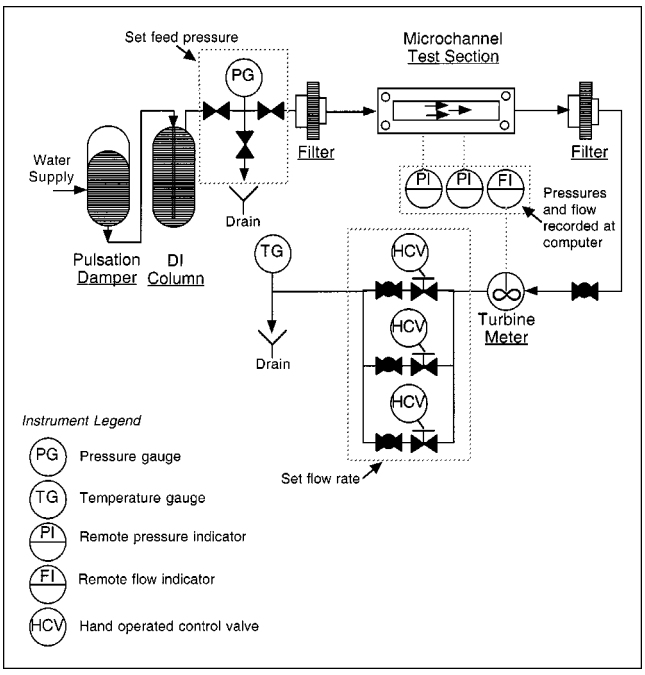

Figure 3. Water flow system.

Upstream and downstream pressure sensors were installed at tap positions 3.048 cm away from the inlet and outlet, respectively, of the microchannel. The distance between the sensors was 4.064 cm. The pressure sensors were located far enough away from the ends of the channel so that a measured pressure drop could be obtained that did not include entrance or exit losses. This was verified in separate experiments by installing one transducer in a fixed location, and moving the other down the length of the channel to obtain a pressure profile at a fixed flow rate. The pressure drop is shown in Figure 4 (in bar/cm) in a 263 μm deep channel vs. distance from the channel inlet (in cm) at a fixed flow rate of 685 mL/min (Re = 2,336). The values in the figure were obtained by numerically differentiating a time-averaged pressure profile curve. At these conditions, the pressure drop in the first 2-cm of the channel, the inlet region, was less than 0.1 bar/cm. The pressure drop in the last 2-cm of the channel was greater than 0.1 bar/cm. The pressure drop was approximately 0.1 bar/cm in the middle 6 cm of the channel. To within the accuracy of this particular experiment, the distance between the taps was not an important factor, outside of the entrance and exit regions. This implies that the taps did not influence the measurement, as any such influence would likely be a decreasing function of the tap-to-tap distance. For all determinations of friction factor, the sensors were installed across the middle 4.064-m of the channel, 59 to 238 times the channel depth (H) away from flow disturbances. Chen (1973) gave a theoretical estimate of entrance length (L) in laminar flow between parallel plates, assuming a uniform inlet profile. L/H was approximately $0.0265^{*}Re$, where the Reynolds number is based on the hydraulic diameter. Thus, at $Re = 2{,}200$ and H = 521 μm, L is 3.037 cm. This value would be a maximum entrance length for all of our microchannel experiments.

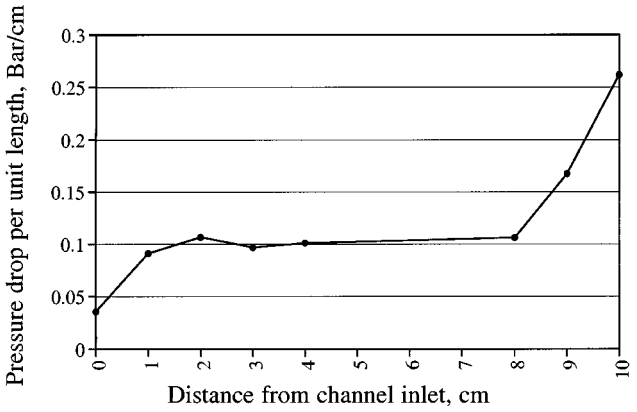

Figure 4. Pressure drop profile in a 263 μm deep channel.

Smooth bottom plate, $Re = 2{,}336$.

The offset between the two pressure sensors was measured for each experiment and was then substracted from each recorded pressure drop. The offset varied from experiment to experiment (possibly from variations in their mounting torque or electrical environment), and was often of the same order of magnitude as the pressure drop. The offset was measured by two methods: (1) By stopping the flow and measuring the difference between the indicated upstream and downstream pressures (the result being averaged over several minutes); (2) By the intercept of the linear pressure drop vs. the flow rate curve obtained in the laminar flow regime. The two values always agreed to within their respective confidence intervals. The offsets (which were averages) ranged between 0.001 bar $+/-$ 0.00006 bar (error on the mean at the 95% confidence level) to 0.0146 bar $+/-0.00003$ bar for the experiments done in the five microchannel configurations.

Experiments were run from high to low flow. Valves were set to give the maximum attainable flow rate through the channel, which also gave the lowest pressure at the downstream sensor. Flow was reduced in increments of approximately 10—25 mL/min, with the valves being adjusted to maintain the pressure at the downstream sensor at the initial minimum value. For the 1,050 μm-deep control, experiments run from both high flows to low and from low flows to high. The two sets of experiments had identical results. Averaged data were logged every second for 3—10 min at each flow rate. Temperatures were recorded every 15 min during each experiment. Temperatures changed slowly, so the temperature at any instant was never more than 0.5°C from the recorded value. Pressure transducer offsets (which were installation-dependent) were always measured (by method 1) at the end of each experiment, after measuring pressure drops at low flows. The pressure difference between the two transducers was linear with flow rate in the laminar regime, and was always continuous, indicating that offset was constant during each experiment. The majority of the experiments were done from high flow to low flow just in case the offset drifted during the course of the experiment. It never did. The control experiment was run both ways with no hysteresis observed.

The Reynolds number (Re), friction factor (f), and friction constant ($f \cdot Re$) were calculated for each logged data point.

Reynolds numbers were calculated based on the mean hydraulic diameter of the channel

$$Re = \frac{D_{eq} v \rho}{\mu},$$

$$D_{eq} = \frac{2\overline{H}}{\left[\left(\frac{\overline{H}}{W}\right) + 1\right]},$$

and $v = q/(\overline{H}W)$, where q is the volumetric flow rate and the channel width $W = 1$ cm.

The Fanning friction factor is defined in the usual way

$$f = \left(\frac{1}{4}\right)\left(\frac{\Delta P}{\frac{1}{2}\rho v^2}\right)\frac{D_{eq}}{L}.$$

In the classical theory, the friction constant for developed laminar flow is a function of aspect ratio and is independent of Reynolds number (Shah and London, 1978). The experimental friction constant was plotted vs. *Re* for each microchannel configuration. Regions of Reynolds number corresponding to laminar flow were identified with portions of the graph having zero slope. Similarly, the regions of turbulent flow were identified with portions of the graph having positive slope, approaching a constant slope at high *Re* corresponding to fully turbulent flow in a rough channel. The identifications were confirmed, in one configuration, with a Reynolds's dye experiment (described below). In earlier work (Peng et al., 1994a, b), discontinuities were observed in plots of friction factor vs. *Re*, and these discontinuities were thought to be associated with the laminar/turbulent transition. In this work, which features closely spaced data points with very little scatter, no such discontinuities were observed.

Error analysis

The combined error in $f \cdot Re$, for high aspect ratio channels, can be approximated by (Holman, 1978)

$$\frac{\delta(\overline{f \cdot Re})}{\overline{f \cdot Re}} = \pm \left\{ \left(3\frac{\delta\overline{H}}{\overline{H}}\right)^2 + \left(\frac{\delta\overline{q}}{\overline{q}}\right)^2 + \left(\frac{\delta\overline{\mu}}{\overline{\mu}}\right)^2 + \left[\frac{\delta(\overline{\Delta P/L})}{\overline{\Delta P/L}}\right]^2 \right\}^{1/2},$$

The over-barred quantities denote mean values. This expression illustrates how uncertainties in instrument calibrations and physical constants propagate into the calculated friction constant. Another source of uncertainty, sampling error, was negligible in comparison to the calibration error. In the above expression, $\delta\overline{H}$ denotes the uncertainty in the mean depth of the channel, values of which were listed in Table 1. $\delta\overline{q}$ is the uncertainty in the mean flow meter calibration curve, which is $+/-0.2$ mL/min (at the 95% confidence level) for the model 102-3P meter and $+/-3.2$ mL/min for the model 102-6P meter, as discussed above. $\delta\overline{\mu}$ is the uncertainty in the mean viscosity, which in turn results from the 0.5°C uncertainty in the temperature. $\delta\overline{\mu}/\overline{\mu}$ is approximately $+/-0.0132$. $\delta(\overline{\Delta P/L})$ is the uncertainty in the mean offset between the two pressure transducers divided by the constant length (4.064 cm). Because of the large number of samples, the uncertainty in the mean ranged between $+/-0.75$ and $+/-38$ millibar/meter, depending on the experiment as discussed above. The most significant source of error for the five microchannel configurations was the uncertainty in the mean depth of the channel. The most significant source of error for the 1,050 μm-deep control was the uncertainty in the mean pressure drop per unit length (which was approximately 5.4% at a flow of 200 mL/min).

The friction constant is not a linear function of the random variables, and not all of the variables could be assumed to have normal distributions. These nonidealities call into question the accuracy of the above RMS formula. For confirmation, a more elaborate procedure was used to estimate the uncertainties in the mean friction constants. Our final estimates of the errors for the different microchannel configurations were made with a Monte-Carlo simulation (Press et al., 1992). The measured means and standard deviations for the variables of channel depth, flow rate, and pressure drop were used to generate normal distributions. Viscosity measurements were assigned uniform distributions with the measured means and with widths given by the 0.5°C uncertainty in the temperature. The resulting distributions were combined to give distributions for the calculated friction constant $f \cdot Re$. The resulting uncertainties were taken to be 1.96 times the standard deviation of the simulated $f \cdot Re$. The maximum uncertainty at the low flow, low pressure drop limit for each experiment is listed in Table 2. The totals range between $+/-5.4\%$ and $+/-11.1\%$. The percentage uncertainties from the simulation were very slightly lower than those determined from the above RMS equation (by between 0.4 and 1.2 percentage points).

Final values for the errors in the Reynolds number were estimated from the distributions for each variable as discussed above. The resulting maximum uncertainties in *Re* are between $+/-1.6\%$ and $+/-3.4\%$ at the low flow limit of each experiment. The particular values for each experiment are listed in Table 2. The uncertainty in the Reynolds number at high flow rates can be approximated by the uncertainty in the viscosity (as the uncertainty in the density was small and of the order of $+/-0.01\%$). The limiting minimum uncertainty (at high flow rates) in *Re* was approximately $+/-1.3\%$.

Table 2. Uncertainties in Measured Friction Constants and Reynolds Numbers (95% Confidence Level)

Exp. μm Deep/ Bottom Plate	$\delta(\overline{f \cdot Re})/\overline{f \cdot Re} \times 100\%$	$\delta(\overline{Re})/\overline{Re} \times 100\%$
1,050/Smooth	±6.5 @ 200 mL/min	±2.1 @ 200 mL/min
521/Smooth	±5.4 @ 100 mL/min	±3.2 @ 100 mL/min
263/Smooth	±8.8 @ 100 mL/min	±3.2 @ 100 mL/min
257/Rough	±8.4 @ 100 mL/min	±3.2 @ 100 mL/min
128/Smooth	±11.1 @ 100 mL/min	±3.2 @ 100 mL/min
128/Smooth	±10.7 @ 15 mL/min	±1.6 @ 15 mL/min

Video photomicroscopy

A particular emphasis of this work was to complement the pressure drop measurements with qualitative observations of flow regimes within the channel. The clear top surface of the channel allowed the fluid to be viewed under a microscope. Dye streams were observed to determine if the flow was laminar or turbulent. The fluroescent dye was a concentrated solution of Rhodamine 6G, which was injected into the microchannel through a pressure tap hole. The absorbance and emission spectra of Rhodamine 6G are broad, with maxima at roughly 525 nm and 555 nm, respectively. A syringe pump injected the dye at a maximum rate of approximately 5 mL/min. A Q-switched, frequency doubled Nd: YLF laser (operating at a wavelength of 534 nm) was used as the light source (to excite the dye), which essentially flooded the viewfield of the microscope. A pair of mirrors was used to direct the beam into the top of the test section. The laser was pulsed at a frequency of 500 Hertz. Scattered green light from the laser that entered the microscope was removed with a low-pass filter (an orange filter with a nominal cutoff wavelength of 550 nm) mounted within the body of the microscope. The fluorescent yellow light emitted from the dye was passed to a CCD-based video camera mounted on the microscope. The camera was operated in its ''high resolution'' mode, wherein entire frames were read altogether at 30 Hz. The camera's electronic shutter was operated at a speed of 1/500 s. Images were recorded on a laser videodisk recorder. Images were then captured later on a Power Macintosh computer model 8100/80AV running the image processing program NIH Image version 1.61 (public domain software from the National Institute of Health). In addition to capturing images, NIH Image was used for preliminary image processing, which in this case was limited to adjusting the brightness and contrast.

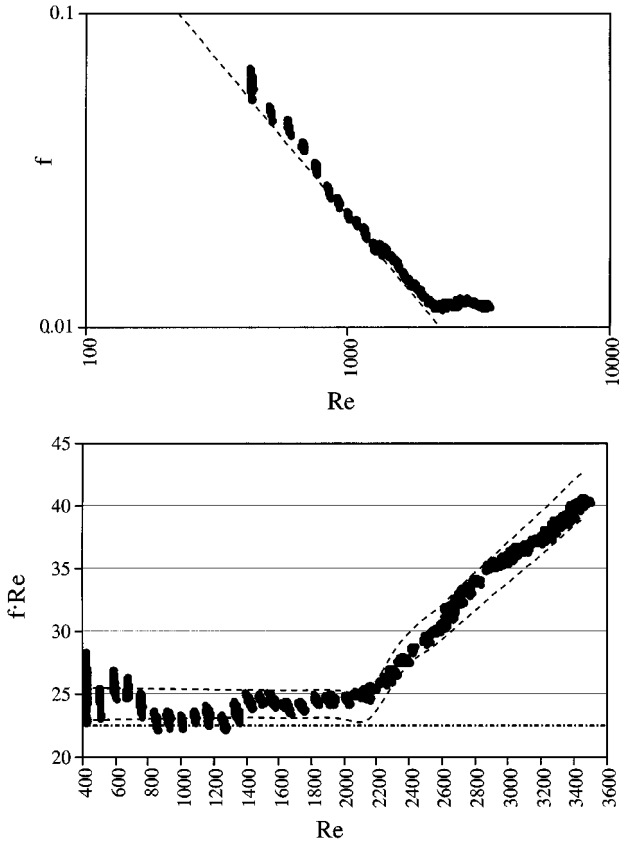

Figure 5. Friction factor and friction constant for a 521 μm deep channel with smooth bottom plate.

Results

Figure 5 shows the friction factor (top half of the figure) and $f \cdot Re$ (bottom half) vs. Re for the 521-μm deep channel with the smooth bottom plate. Each plot includes approximately 7,000 data points (each point being an average over one second) logged at a rate of one point per second. The dashed line in the upper half of the figure is the classical result for developed laminar flow in a duct with an aspect ratio of 19.19:1, namely, $f = 22.4/\mathrm{Re}$ (Shah and London, 1978). In the bottom half, the average of the product $\overline{f \cdot Re}$ remained constant at approximately 24.2 ± 1.3 for Reynolds numbers less than about 2,200. This was the region of laminar flow. The small oscillations seen in $\overline{f \cdot Re}$ with flow at low Re were the result of the slight nonlinearity of the model 102-6P turbine flow meter. The fine dashed lines in the lower half of Figure 5 are the approximate upper and lower bounds on $\overline{f \cdot Re}$, given the uncertainties in the channel depth and other variables as discussed above. The heavy dashed line marks the classical value of 22.4. The measured value of the friction constant was significantly higher than the classical value. The fact that $f \cdot Re$ did not decrease with decreasing Re in the laminar regime confirms that the pressure transducers were sufficiently far away from the entrance and exit of the channel.

As indicated in the upper half of Figure 5, the friction factor became constant at 0.012 at high Reynolds numbers. A constant friction factor indicates fully turbulent flow in a rough conduit. No power law behavior was observed for the turbulent friction factor. The transition to turbulence occurred at the Reynolds number for which $\overline{f \cdot Re}$ began to increase with Re. This is seen, in the bottom half of Figure 5, to be at a Reynolds number of approximately 2,200. As noted by Peng et al. (1994a), the transition to turbulent flow occurs at relatively low Reynolds numbers in microchannels. The lower critical Reynolds number for transition to turbulent flow in parallel plate macrochannels is known to be 2,800 (Hanks and Ruo, 1966). Dye stream experiments were attempted to verify the flow regimes indicated by the measurements of friction factor. Unfortunately, the images were not sharp enough for this channel depth to be useful.

Plotted in Figure 6 are similar results for the 263-μm deep channel with the smooth bottom plate. The friction factor in the low flow, laminar regime was larger than the theoretical result of 23.2-the mean $\overline{f \cdot Re}$ was 26.1 ± 2.3. The fact that the deviation from theory persisted as the channel depth was reduced from 521 to 263-μm indicates that it was not caused by entrance length effects-entrance contributions to the pressure drop must decrease with decreasing channel depth and fixed transducer locations.

For this channel, the product $\overline{f \cdot Re}$ was an increasing function of Re for Reynolds numbers greater than about 1,700 and was constant for lower Reynolds numbers. The transition to turbulence occurred at ever-lower Reynolds numbers as

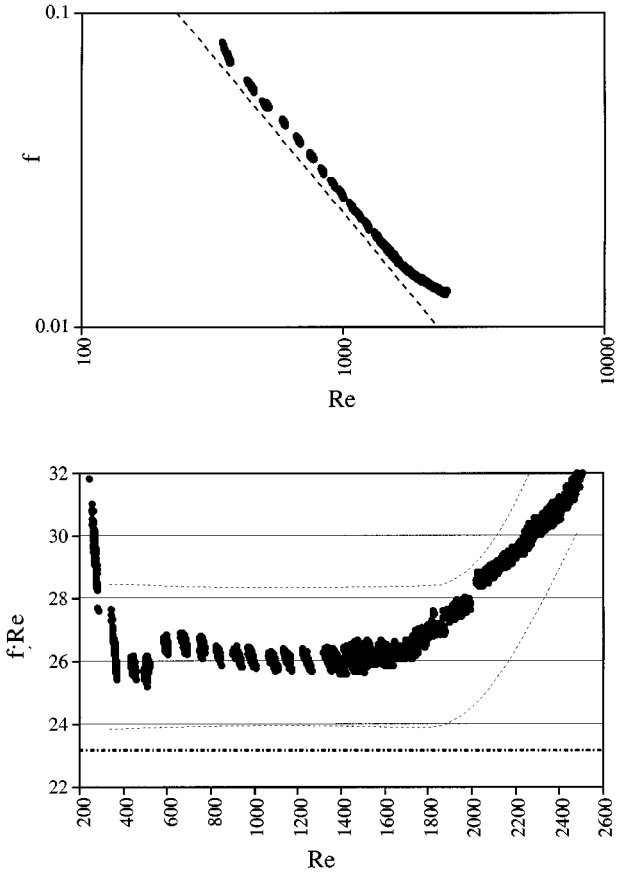

Figure 6. Friction factor and friction constant for a 263 μm deep channel with the smooth bottom plate.

the channel depth was reduced. A dye stream flow visualization experiment was performed to verify that the flow actually was laminar for $Re < 1{,}700$ (in the 263 μm deep channel) and turbulent otherwise. Dye was injected (as discussed above) through a pressure tap positioned 2.032 cm from the inlet of the channel. The tap was 2 mm away from the sidewall of the channel. Images were recorded at a position 5.08-cm downstream from the injection point. Video photomicrographs of the dye stream are shown in Figure 7. The plane of the image is parallel to the microchannel and is positioned mid-channel. Photographs are presented for four different flow rates. In the top left of the figure, the Reynolds number was 1,511. The dimensions of the video frame are approximately 1.88 mm $\times$ 1.41 mm. The width of the dye stream in the image is approximately one-half millimeter-equal to the diameter of the dye injection hole-and the edges of the stream are sharp, indicating little transverse mixing at the low flow rate. The flow was laminar. The dye stream had the same appearance at all lower flow rates. In the upper righthand corner of the figure is an image taken at $Re = 1{,}586$. The image is nearly identical to that taken at the lower flow rate. The flow was still laminar. Increasing the Reynolds number to 1,723 caused the dye stream to expand and become diffuse, showing much more transverse mixing of the dye. The change in the width of the dye stream occurred at approximately the same flow rate as the change in slope of the curve of $f \cdot Re$. This is shown in the bottom lefthand corner of Figure 7. The image taken at $Re = 2{,}064$ (in the bottom right corner of the figure) is similar. The flows shown in this latter pair of images were turbulent. The transition Reynolds number obtained from the plot of $f \cdot Re$ vs. Re agreed with that obtained from the dye stream experiment. The turbulent friction factor approached a value of 0.013 at high Reynolds numbers for the 263-μm deep, smooth microchannel.

Friction factors in laminar flow were increased above the theoretical value when the microchannel was greatly roughened. Plotted in Figure 8 are the results obtained in the 257-μm deep roughened channel. Strong flow oscillations occurred between Reynolds numbers of 400 and 700, as shown in the upper half of the figure; the noise disappeared at higher and lower flow rates and was observed again over the same range of Re in repeat experiments. Values of $f \cdot Re$ for Reynolds numbers above the noise band are plotted vs. Re in the lower half of the figure. The value reached at low Re was approximately 29 ± 2.4, significantly above the classical value of 23.2. The plot may have some slight curvature at lower Re, which suggests that flow is not quite fully developed in a channel as rough as this. Unfortunately, the uncertainty in the friction constant is large enough to encompass any presumed curvature.

For the roughened channel, the Reynolds number for transition to turbulent flow did not appear to shift from the value of 1,700 obtained in the smooth, 263-μm deep channel, although the exact transition point was difficult to determine from friction factor results. The friction factor in the turbulent regime approached a value of 0.016, considerably above the value obtained in the smooth channel.

The smallest channel examined in this study was a 128-μm deep channel assembled with the smooth bottom plate. Results, using this channel, for the friction factor and $f \cdot Re$ are plotted vs. Re in Figure 9. Results are plotted in the figure from two separate experiments, one performed with the high-range flowmeter, the other performed with the low-range flowmeter. The flow was laminar over the range of Reynolds numbers examined. This was verified with a dye stream injection experiment, which showed only a small, coherent dye stream over the whole range of flow rates that were achievable. For this channel, high-pressure drops prevented the high flow rates necessary for turbulence. The average value of $\overline{f \cdot Re}$ at low Re was approximately 26 ± 2.8, which agreed with the classical value of 23.6 within the uncertainty of the experiment. For this small channel, the uncertainty in the depth of ± 5 μ was relatively large, making it difficult to distinguish the measured friction factors from the theoretical value.

Experiments were also performed a 1,050 μm-deep channel that served as a control. Unfortunately, the channel was not long enough, and nor were the pressure transducers accurate enough to obtain reliable results over a broad range of flow rates. For Reynolds numbers less than about 600, uncertainties in the transducer offset were high. For Reynolds numbers higher than about 1,000, there was a possibility of undeveloped flow. The average $\overline{f \cdot Re}$ was 21.8 for Reynolds numbers between 600 and 900, with uncertainties being ± 1.4 at $Re = 600$, and ± 1.0 at $Re = 900$. This result was in rough agreement with the theoretical value of 21.1. However, the offset between the pressure transducers was not reproduca-

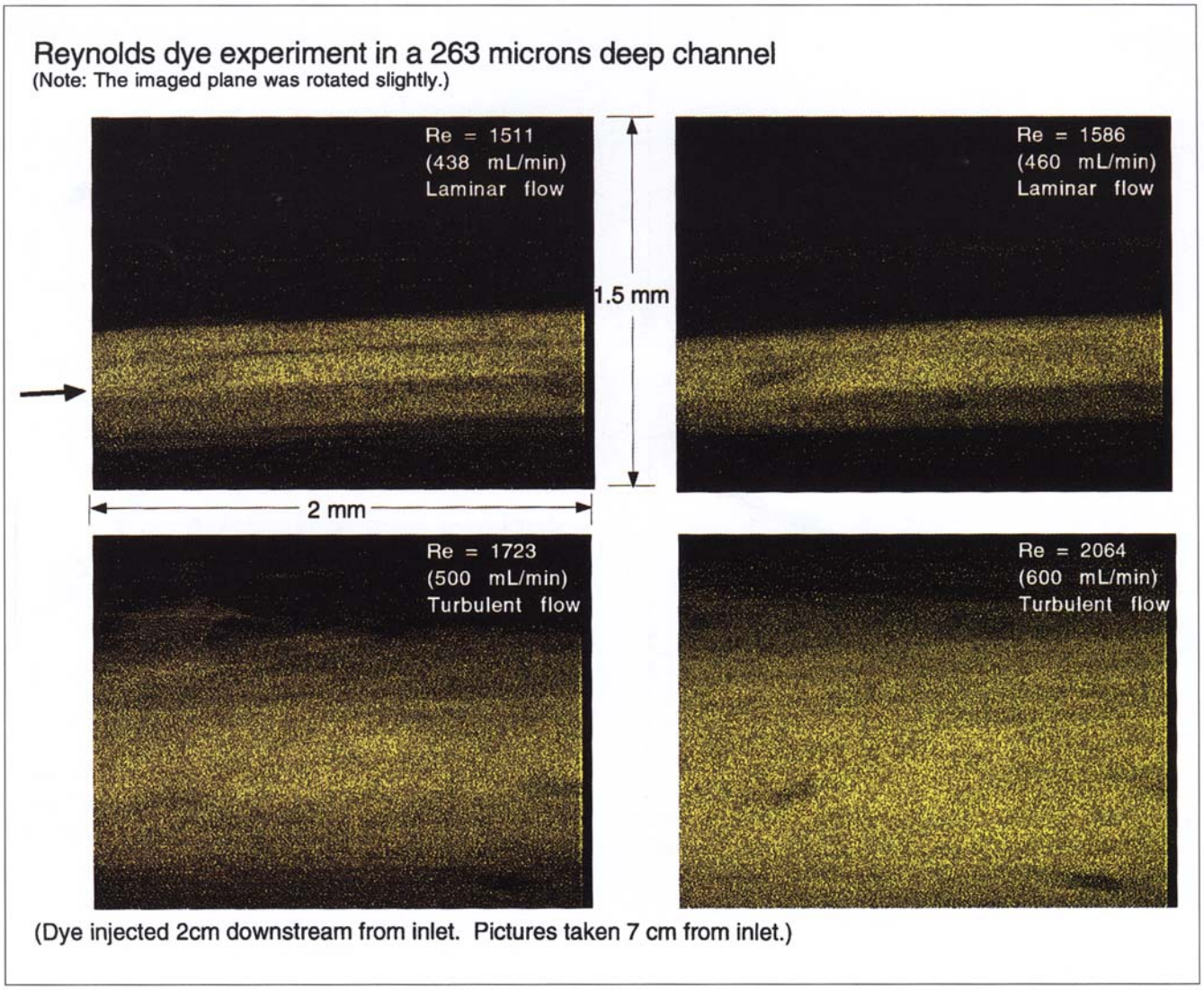

Figure 7. Images of a dye stream in the 263 μm deep channel with the smooth bottom plate.

ble to the accuracy required for these low-pressure drop, macrochannel experiments.

Although each microchannel configuration exhibited significantly higher friction constants than predicted by laminar flow theory, it is not possible to conclude from these data that channel geometry or relative roughness were related to the higher constants. The overlapping of the confidence intervals precludes conclusions about the importance of these parameters. The ranges of possible $\overline{f \cdot Re}$ in laminar flow for each experiment are plotted in bar graph form in Figure 10. The possible treatments of reduction in channel depth at constant roughness, and increase in roughness at constant depth, produced no significant changes in the friction constant.

Summary and Conclusions

Pressure drops were measured, and friction factors were calculated for water flow in approximately 2-D microchannels. Both smooth and rough channels were examined. The surface roughness of each channel was measured over large areas using a white light inteferometer. Pressure drops were evaluated using taps within the channels, far away from the entrance and exit regions. Confidence intervals were determined for each of the measurements made during the experiments, and the propagation of these uncertainties to the derived results was determined. A major source of uncertainty in the friction factors was the relatively wide confidence intervals on the mean channel depths.

For every case but one, friction factors in laminar flow were significantly greater than the classical values. A greatly roughened channel exhibited friction factors in laminar flow which were very much above the theoretically predicted values. Uncertainties in the measured friction factor make it impossible to conclude with confidence that either channel geometry or channel roughness are important factors in determining the friction factor for laminar flow in microchannels. For the smallest channel depth, a high relative uncertainty in the depth made it impossible to distinguish measured friction factors from theory. Friction factors in laminar flow were

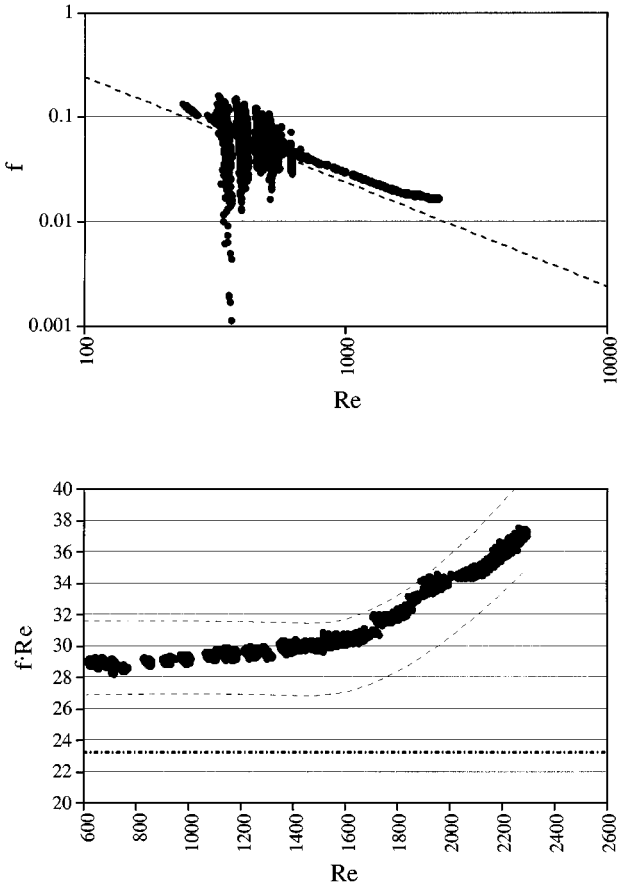

Figure 8. Friction factor and friction constant for a 257-μm deep channel with the rough bottom plate.

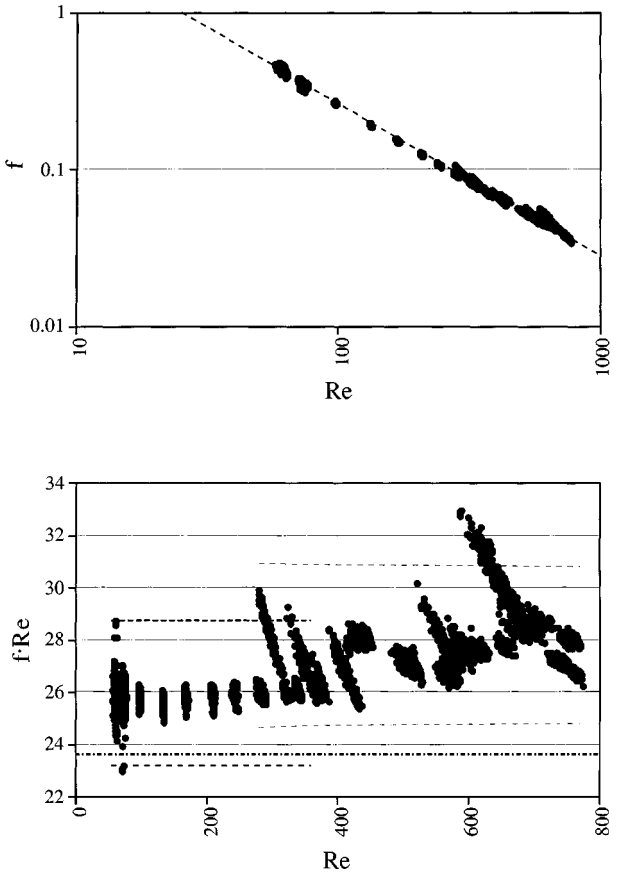

Figure 9. Friction factor and friction constant for a 128-μm deep channel with the smooth bottom plate.

proportional to Re^{-1} to the degree of accuracy of the experiments. High relative roughness may cause the friction constant $f \cdot Re$ to vary with Re. Uncertainties in the measured constant obscure this effect.

Laminar to turbulent transitions were detected from both friction factor and flow visualization experiments. The two techniques yielded similar results. The transition to turbulence occurred at Reynolds numbers that were lower than the critical Reynolds number for macroscopic ducts, and transition Reynolds number decreased further with decreasing channel depth. However, transition Reynolds numbers were much larger than the values of 200—700 that have been reported in the literature. The transition appeared to approach the classical value of 2,800 as depth was increased. The transition when going from laminar to turbulent flow was sudden, but not discontinuous. The continuity suggests eddying around surface features, which gradually increased with increasing flow. Preliminary images that we have taken of low Reynolds number flows seeded with fluorescent particles have shown eddies (in a plane parallel to the channel) near the top of the microchannel, with particle motion being constrained by surface features. Studies of such motion will be the subject of future research.

Recently, similar departures from laminar flow theory were observed for flows of water in trapezoidal silicon microchannels (Weilin et al., 2000). The investigators attributed the increased friction to a ''roughness viscosity''-a concept similar to an eddy viscosity-which increases near the wall. A mecha-

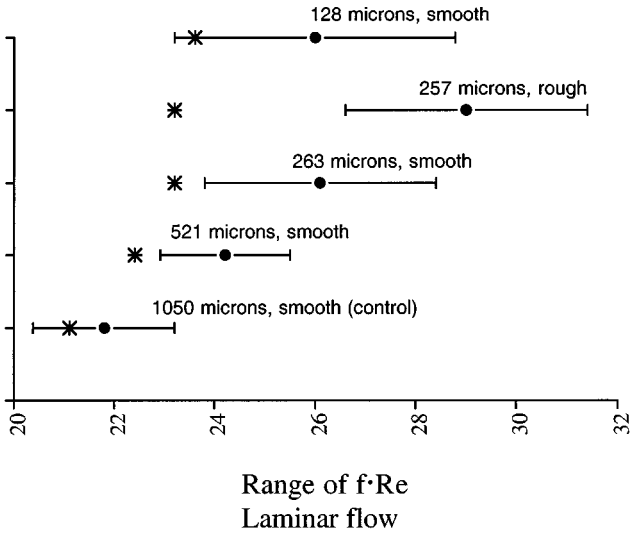

Figure 10. Interval estimates of the friction constants for laminar flow.

* Denotes classical values for developed laminar flow.

nism has not yet been given for such a phenomenon. The concept would seem to be inapplicable to our results as the range of the wall effect would have to be an order of magnitude larger than the feature height to model them. In any case, it is not our intent to claim that we have documented every possible source of excess pressure drop-obviously, we have not. However, having examined the expected sources, the excess remains. To identify the source will require even more refined experiments, coupled with computational studies.

Acknowledgments

This work was supported by Dr. Robert Price of the Division of Engineering and Geosciences, Office of Energy Research, Office of Basic Energy Sciences of the U.S. Dept. of Energy. Battelle Memorial Institute operates Pacific Northwest National Laboratory. The authors wish to thank W. D. Bennett and M. White of Pacific Northwest National Laboratory for their work in the design and fabrication of the test section, P. M. Martin, J. M. Cuta, and M. Friedrich for helpful discussions on the design of the test section and flow loop, G. C. Dunham for help with the use of the Zygo Profilometer, and B. J. Palmer for advice on statistics.

Literature Cited

Arkilic, E. B., M. A. Schmidt, and K. S. Breuer, ''Gaseous Slip Flow in Long Microchannels,'' *J. of Microelectromechical Systems*, **6**, 167 (1997).

Chen, R.-Y., ''Flow in the Entrance Region at Low Reynolds Numbers,'' *J. Fluids Eng.*, **95**, 153 (1973).

Cuta, J. M., C. E. McDonald, and A. Shekarriz, ''Forced Convection Heat Transfer in Parallel Channel Array Microchannel Heat Exchanger,'' *ASME Proc. PID-Vol. 338 Advances in Energy Efficiency, Heat/Mass Transfer Enhancement*, pp. 17—23 (1996).

Delly, J. G., *Photography Through the Microscope*, 9th ed., Eastman Kodak Company, Rochester, NY (1988).

Hanks, R. W., and H. Ruo, ''Laminar-Turbulent Transition in Ducts of Rectangular Cross Section,'' *I& EC Fundam.*, **5**, 558 (1966).

Holman, J. P., *Experimental Methods for Engineers*, McGraw-Hill, New York (1978).

Kleiner, M. B., S. A. Kuhn, and K. Haberger, ''High Performance Forced Air Cooling Scheme Employing Microchannel Heat Exchangers,'' *IEEE Trans. on Components, Packaging, and Manufacturing Technology-Part A*, **18**, (4), 795 (1995).

Knight, R. W., D. J. Hall, J. S. Goodling, and R. C. Jaeger, ''Heat Sink Optimization with Application to Microchannels,'' *IEEE Trans. on Components, Hybrids, and Manufacturing Technology*, **15** (5), 832 (1992).

Mendenhall, W., and T. Sincich, ''Statistics for the Engineering and Computer Sciences,'' Dellen, San Francisco (1984).

Peng, X. F., G. P. Peterson, and B. X. Wang, ''Frictional Flow Characteristics of Water Flowing Through Rectangular Microchannels,'' *Exp. Heat Transfer*, **7**, 249 (1994a).

Peng, X. F., G. P. Peterson, and B. X. Wang, ''Heat Transfer Characteristics of Water Flowing Through Microchannels,'' *Exp. Heat Transfer*, **7**, 265 (1994b).

Pfahler, J., J. Harley, H. H. Bau, and J. Zemel, ''Liquid Transport in Micron and Submicron Channels,'' *Sensors and Actuators*, **A21**—**A23**, 431 (1990a).

Pfahler, J., J. Harley, H. H. Bau, and J. Zemel, ''Liquid and Gas Transport in Small Channels,'' *ASME Proc., DSC*, Vol. 19, Winter Annual Meeting, Dallas, 149 (1990b).

Pong, K., C. Ho, J. Liu, and Y. Tai, ''Non-linear Pressure Distribution in Uniform Microchannels,'' *ASME FED-Vol. 197*, **51** (1994).

Press, W. H., S. A. Teukolsky, W. T. Vettering, and B. P. Flannery, ''Numerical Recipes in C,'' Cambridge University Press, New York (1992).

Schlichting, H., *Boundary-Layer Theory*, McGraw-Hill, New York (1979).

Shah, R. K., and A. L. London, *Laminar Flow Forced Convection in Ducts*, Academic Press, New York (1978).

Weilin, Q., M. Mala, and L. Dongqing, ''Pressure-driven Water Flows in Trapezoidal Silicon Microchannels,'' *Int. J. of Heat and Mass Trans.*, **43**, 353 (2000).

Wu, P., and W. A. Little, ''Measurement of Friction Factors for the Flow of Gases in Very Fine Channels Used for Microminiature Joule-Thomson Refrigerators,'' *Cryogenics*, **23**, 273 (1983).

Yu, D., R. Warrington, R. Barron, and T. Ameel, ''An Experimental and Theoretical Investigation of Fluid Flow and Heat Transfer in Microtubes,'' *Proc. of the ASME/JSME Thermal Eng. Joint Conf.*, Maui, HI, **1**, 523 (1995).

Manuscript received Jan. 27, 1999, and revision received Feb. 25, 2000.